Soft Matter

PAPER

Cite this: *Soft Matter*, 2018, **14**, 992

Capture of colloidal particles by a moving microfluidic bubble†

Irma Liascukiene,[a] Gabriel Amselem,[a] Deniz Z. Gunes[b] and Charles N. Baroud*[a]

Received 29th November 2017,
Accepted 7th January 2018

DOI: 10.1039/c7sm02352a

rsc.li/soft-matter-journal

Foams can be stabilized for long periods by the adsorption of solid particles on the liquid–gas interfaces. Although such long-term observations are common, mechanistic descriptions of the particle adsorption process are scarce, especially in confined flows, in part due to the difficulty of observing the particles in the complex gas–liquid dispersion of a foam. Here, we characterise the adsorption of micron-scale particles onto the interface of a bubble flowing in a colloidal aqueous suspension within a microfluidic channel. Three parameters are systematically varied: the particle size, their concentration, and the mean velocity of the colloidal suspension. The bubble coverage is found to increase linearly with position in the channel for all conditions but with a slope that depends on all three parameters. The optimal coverage is found for 1 μm particles at low flow rates and high concentrations. In this regime the particles pass the bubbles through the gutters between the interface and the channel corners, where the complex 3D flow leads them onto the interface. The largest particles cannot enter into the gutters and therefore provide very poor coverage. In contrast, particle aggregates can sediment onto the microchannel floor ahead of the bubble and get swept up by the advancing interface, thus improving the coverage for both large and medium particle sizes. These observations provide new insight on the influence of boundaries for particle adsorption at an air–liquid interface.

1 Introduction

Liquid foams are inherently out-of-equilibrium systems that are nevertheless ubiquitous in everyday life and industrial settings. Among the many ways that have been devised to slow down their aging, the adsorption of solid particles onto the liquid–air interfaces[1,2] has attracted strong attention in recent years.[3,4] This approach is of special interest to the industry for two reasons: (i) the particles confer extra stability, including for non-aqueous systems,[5] when they replace or are combined with molecular surfactants; (ii) particles can represent a natural alternative to molecular emulsifiers, in particular in the food area.[6]

Solid particles play a similar role as surfactants since a particle that adsorbs onto an interface reduces the total free energy of the liquid–solid–gas system for any contact angle other than full wetting.[7] Since the energy gain due to this adsorption is orders of magnitude larger than thermal fluctuations, particles tend to remain adsorbed once they reach the interface, unlike molecular surfactants.[8] This equilibrium picture however does not address the question of getting the particles onto the interface, which requires the system to overcome energetic barriers such as electrostatic repulsion between the interface and the particle, the resistance of the lubrication film to drainage, or the forced dewetting of the initial suspension liquid at the contact with the particle.[3]

Indeed the adsorption process comprises multiple steps: collision between the particle and the bubble, attachment to the interface and, potentially, detachment.[9] While attachment and detachment are controlled by both hydrodynamics and the physical chemistry of the system,[3,9] collision has a purely hydrodynamic origin.[9,10] These processes have been extensively studied in the context of froth flotation[9–16] but mostly by considering a particle adsorbing onto a single bubble[17,18] far from other solid or liquid interfaces.

Recently, the advent of microfluidics has enabled the controlled production of bubbles covered by particles, sometimes called armored bubbles. This can be achieved either at high flow rates in which inertial effects push the particles onto the interface,[19–21] or at low flow rates by squeezing the particles into the thin film between the gas–liquid interface and a solid wall.[22,23] Similar physical mechanisms can be found in industrial processes: while the whipping of a liquid suspension at high average Reynolds number at kitchen or industrial scale would involve large inertial effects, the whipping of a colloidal gel at lower Reynolds

[a] *Laboratoire d'Hydrodynamique, Ecole Polytechnique, 91128 Palaiseau Cedex, France. E-mail: baroud@ladhyx.polytechnique.fr; Tel: +33 1 69 33 52 61*
[b] *Nestlé Research Center, Institute of Material Science, Vers-chez-les-Blanc, CH-1000, Lausanne 26, Switzerland*

† Electronic supplementary information (ESI) available. See DOI: 10.1039/c7sm02352a

number, *e.g.* below the turbulent regime, would involve particles being squeezed between two bubbles, or between a bubble and a solid boundary.

In contrast with large-scale foaming methods however, microfluidics allows the production of armored bubbles while independently tuning the bubble size and the time during which colloidal particles adsorb onto the interface. It also provides optical access to observe the kinematics of the coverage process.[22,24,25] These properties were used by Kotula and Anna,[22] who probed the adsorption dynamics of nanometric particles at the liquid/air interface in a microfluidic channel, reporting that particle adsorption could lead to bubble break-up in the channel. Similarly, Zoueshtiag *et al.*[24] investigated the influence of different wetting configurations for the particles and the channel walls on the formation of an armored bubble within a microfluidic device. Finally, Yu *et al.*[23] considered the interactions between the particle adsorption and the lubrication film between the bubble and tube wall.

Here we use the same device as Taccoen *et al.*[25] to measure the dynamics of colloidal particle adsorption onto the interface of a bubble flowing in a microchannel. The influence of three parameters is studied: the particle size, the particle concentration in the suspension, and the speed at which the bubble is pushed through the device. We first address the hydrodynamic questions through the relative velocity of the bubble and the outer fluid. Then we find that particles can adsorb to the bubble interface by two distinct routes: small particles reach the interface as they pass the gutters between the bubble and the channel walls, while large aggregates tend to sediment onto the channel floor where the interface captures them as the bubble passes by. The final coverage decreases with increasing flow speed, and increases when particles have had time to aggregate.

2 Material and methods

2.1 Colloidal particles

FluoSphere® carboxylate-modified 0.5 and 1.0 μm polystyrene microspheres were purchased from Molecular Probes/Life Technologies (Grand Island, NY), 4.5 μm Fluoresbrite™ carboxy microspheres were purchased from Polysciences Inc. (Warrington, PA). Concentrations ranging between 0.1–1.0 wt% of solids (Table 1) were prepared in an aqueous solution of 0.5 M NaCl (Analytical, NormaPur, 99.5% min) in Milli-Q water.

The concentrations in suspension were varied according to Table 1, where the weight and number concentrations are reported for all of the experimental conditions.

Table 1 Particle sizes and colloidal concentrations used in the coating experiments

	$c_{particles}$ (particles per mL)		
c, wt%	d = 0.5 μm	d = 1.0 μm	d = 4.5 μm
0.1	1.46×10^{10}	1.82×10^{9}	2.05×10^{7}
0.5	7.28×10^{10}	9.09×10^{9}	1.03×10^{8}
0.8		1.46×10^{10}	
1.0		1.82×10^{10}	

2.2 Microfluidic design

The microfluidic device was produced by soft lithography, by first producing a brass mold using a CNC micromilling machine (Minitech Machinery Corporation, USA), following a 3D model of the channel drawn under a CAD software (RhinoCAM, Rhinoceros, McNeel Europe). Liquid PDMS (Sylgard 184, Dow Corning, USA) with curing agent at a ratio of 1 : 10 was then cast over the mold and cured on a hot plate at 150 °C for at least 24 h. This thermal aging was necessary to reduce the hydrophobic recovery of the PDMS after plasma treatment.[26] The patterned PDMS was sealed to a glass slide after 35 s of plasma treatment (Harrick Plasma, USA), and the resulting channel was immediately filled with distilled water (Milli-Q, Merck, Germany) to ensure walls hydrophilicity. The microfluidic chips were stored in a 100% humidity sealed container in order to prevent drying and to keep the channels hydrophilic.

The microfluidic device had two inlets and two outlets. The inlets were connected to a liquid and air filled syringes, controlled by a syringe pump (Nemesys, Cetoni). In turn, the outlets were connected to a controlled pressure source (MFCS, Fluigent). The geometry consisted of three successive regions: One for bubble creation, followed by a "coating" channel for particle adsorption, and a final dome-shaped chamber for bubble monitoring (see Fig. 1). The device was placed on an inverted microscope (Nikon Eclipse Ti-U) and images were acquired using a Photron Fastcam SA3 camera. Images were analyzed using Fiji[27] and custom Matlab code (The MathWorks, Inc., USA).

2.3 Experimental protocol

In a typical experiment a syringe containing the colloidal suspension was connected to the first inlet and the entire device was pre-filled with the colloidal suspension. Then, a syringe filled with air was connected to the second inlet. Experiments began when an air bubble was created quasi-statically in the first region through the use of a confinement gradient[25,28] in roughly 30 seconds to 1 minute, letting very little time for the colloids to aggregate. Typical bubble volumes in our experiments were 23 nL, which corresponded to a length of approximately 1 mm in the coating channel.

Once the bubble was created, a flow of the colloidal suspension was imposed, forcing the air bubble to travel through the

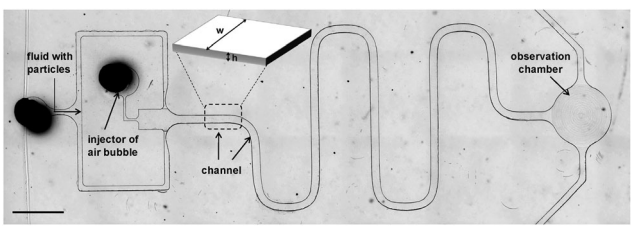

Fig. 1 An optical microscope image of the microfluidic device. The two inlets on the left hand side allow the injection of the air and the aqueous solution. The observation chamber on the right hand side has a dome-shaped cross-section and is connected to a pressure controller through the two outlet channels. A more detailed description of the 3D shape is given in ref. 25. Dimensions are h = 78 μm, w = 300 μm. Scale bar is 2 mm.

Table 2 List of the flow rates Q used throughout the study, together with the corresponding average fluid velocities $U = Q/(w \times h)$, and capillary numbers Ca

Q (μL min^{-1})	U ($\times 10^{-3}$ m s^{-1})	Ca ($\times 10^{-4}$)
0.5	0.36	0.051
1.0	0.71	0.10
1.5	1.07	0.15
2.0	1.42	0.20
5.0	3.56	0.51
10.0	7.12	1.0

rectangular coating channel. The flow rates Q used in this study are listed in Table 2, together with the corresponding average fluid velocities $U = Q/(w \times h)$, and the capillary number $\mathrm{Ca} = \eta U/\gamma$. Using $\eta = 10^{-3}$ Pa s for the dynamic viscosity of water and $\gamma = 7 \times 10^{-2}$ N m^{-1} for the interfacial tension between air and water, Ca was in the range $[0.051\text{–}1.0] \times 10^{-4}$. The flow profile in the coating channel in the absence of a bubble is shown in Fig. S1 (ESI†).

3 Experimental observations

3.1 General overview

Typical fluorescence micrographs of a bubble being transported through the channel are shown on Fig. 2A–H. They show a bubble entering the coating channel and flowing from left to right towards the exit. The gradual adsorption of particles on the interface is visible from the fluorescent intensity of the bubble, which begins dark (no adsorbed particles) and gradually becomes bright (many adsorbed particles). Therefore the variation in fluorescent intensity of the bubble is an indicator for the adsorption of particles on the interface.

Information about the bubble's evolution can be summarized on a single kymograph, which displays the fluorescence intensity along the channel centerline as a function of time, as shown in Fig. 2I. Two signatures of particle adsorption onto the air/liquid interface are apparent on the kymograph. First, the brightness of the bubble increases with time. Second, the fluorescence of the solution is higher upstream than downstream of the bubble, indicating that the concentration of particles in solution is higher upstream of the bubble – *i.e.* on the left-side of the kymograph – than downstream. Note that the fluorescence intensity of the depleted region is non zero, indicating that not all particles are adsorbed onto the interface. Moreover, the size of the depleted region grows with time, as a result of the speed differential between the bubble and the particles in the channel centerline. A more thorough analysis of the depleted region is given in Section 4.4.

3.2 Bubble speed

The speed of a drop or bubble advected by an outer fluid in a rectangular microfluidic channel depends on many parameters, such as the aspect ratio of the channel, the size of the droplet, the capillary number, and the viscosity ratio between the continuous and discontinuous phases.[29,30] Moreover, the presence of particles at the interface could potentially influence the speed of the bubble.

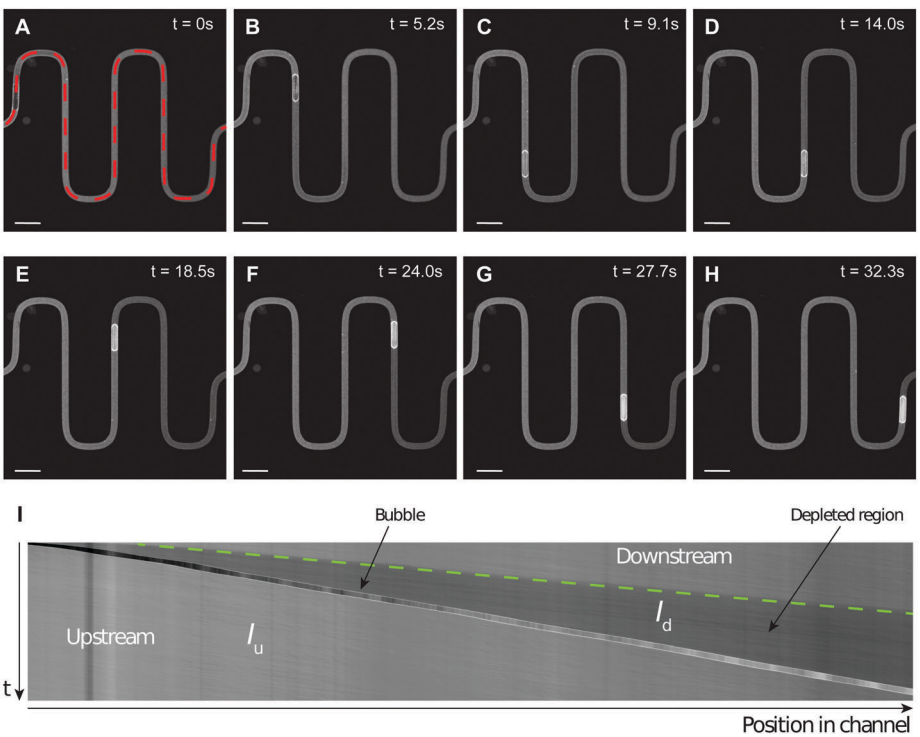

Fig. 2 (A)–(H) Time-lapse of a bubble flowing through the coating channel. Flow speed: $U = 0.71$ mm s^{-1}. Colloidal suspension: 0.5 wt% 1.0 μm particles. Scale bars: 1 mm. The centerline of the channel is indicated by the dashed red line. (I) Kymograph showing the evolution of the fluorescence intensity along the channel centerline (x-axis) as a function of time (y-axis). Time goes from top to bottom. Flow is from left to right. Particles adsorb onto the bubble interface, which appears as two bright lines. Upstream of the bubble, the average fluorescence value is I_u. Downstream of the bubble, the fluid is depleted in particles and has an average fluorescence value I_d. The front of the depleted region is highlighted by the green dashed line.

In our devices the bubble speed was evaluated at different locations and found to be constant throughout the channel (Fig. S2, ESI†), always matching the mean velocity U of the liquid, defined as $U = Q/A$, where Q is the imposed fluid flow rate and A the channel cross-sectional area (see Fig. S2, ESI†). These measurements were consistent with results reported by Fuerstman *et al.*[31] and more recently by Jakiela *et al.*,[29,30] in spite of the difference in aspect ratios and bubble lengths between the different conditions. It is noteworthy that the bubble velocity did not depend on the presence of particles at the interface in our conditions, even for high surface coverage, in contrast with surfactant covered bubbles.[31]

The residence time τ of the bubble in the coating channel was therefore directly linked to U through $\tau = L/U$, where $L = 32$ mm is the length of the channel. Varying the flow rates produced residence times between 5 and 90 s in the coating region.

3.3 Zooming in on a bubble

Zooming in on a moving bubble provides indications on the mechanism of adsorption, as shown in Movies S1 and S2 (ESI†). These movies show that colloidal particles in the central region of the channel catch up with the bubble and are diverted towards the gutters at the sides of the bubble, as sketched by the black particle in Fig. 3A. The particles seem to adsorb on the front of the bubble (*i.e.* region facing the outlet) as they exit the gutters downstream of the bubble. Once adsorbed on the interface the particles recirculate toward the channel floor and ceiling, where they are trapped in the lubrication film between the bubble and the walls, as indicated by the red particles in Fig. 3A and B. As the bubble back (*i.e.* interface facing towards the inlet) passes over these trapped particles, the colloids remain at the bubble interface and recirculate again towards the front. These observations are consistent with PIV results for the flow around a bubble in a rectangular microfluidic channel,[32,33] and for the recirculation along a droplet interface.[34]

Therefore, two different mechanisms of adsorption are at play and complement each other. On the one hand, particles in the bulk suspension enter into the gutters and can adsorb onto the interface in the gutters, or at the bubble front. On the other hand, particles already at or near the channel walls will adsorb onto the interface at the bubble back. We investigate both mechanisms in the following.

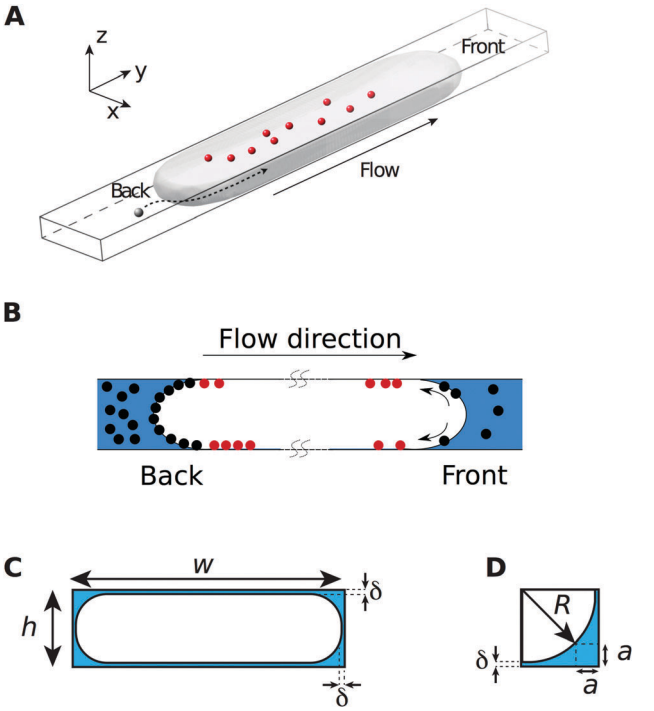

Fig. 3 (A) Sketch of a bubble flowing in the microchannel. Colloidal particles traveling faster than the average flow speed catch up with the bubble, and are diverted towards the gutters between the bubble and the channel corner (black bead). They are captured at the interface in the gutters or at the bubble front. Particles trapped in the lubrication film (red beads) adsorb on the interface. (B) Side view of a bubble: particles trapped at the interface at the front of the bubble (black) recirculate towards the channel floor or ceiling. They are then trapped in the lubrication film (red beads). Then, as the bubble passes over them, they become trapped at the bubble back. (C) Bubble shape in the coating channel, cross-section view. The lubrication film has a thickness δ. The bubble is rounded, leaving space for gutters (in blue) between its curved interface and the channel walls. (D) Zoom on the corner region, showing the typical gutter size a. We estimate $a \simeq 9$ μm in our channels.

4 Adsorption in the gutters

We now turn to measurements of particle adsorption on the interface as the three experimental parameters are varied: first the particle concentration, then the particle size, then the flow velocity.

4.1 Influence of the particle concentration

The coverage of the bubble interface increased as the bubble advanced in the coating channel, as evidenced by an increase in the fluorescence of the interface. For 1.0 μm particles at a concentration of 0.1 wt%, the fluorescence intensity increased linearly with the bubble position (see Fig. S3, ESI†). In contrast, at higher concentrations of 0.5 and 0.8 wt%, the surface coverage first increased with the bubble position, then saturated and reached a plateau towards the end of the coating channel, an indication that the interface was becoming crowded with particles. These results were similar for all flow speeds and particle sizes that were tested, see Fig. S4 (ESI†).

4.2 Influence of the particle size

Three different particle diameters were used in our study: 0.5, 1 and 4.5 μm. The behavior of these particles depends on their size relative to two characteristic length scales in the experiment, namely the size of the gutters (a) and the thickness of the lubrication film (δ), as sketched in Fig. 3C and D.

In the range of capillary numbers used in our study ($\mathrm{Ca} = [0.051\text{–}1.0] \times 10^{-4}$), the radius of curvature R in the corners of the bubble is prescribed, to leading order, by the channel geometry:[22]

$$R = \frac{h + w - \sqrt{h^2 + w^2 + (\pi - 2)hw}}{4 - \pi}, \qquad (1)$$

so that $R \approx 32$ μm. The typical size of the gutter is therefore given by $a \approx (\sqrt{2}-1)/\sqrt{2}R \approx 9$ μm, see Fig. 3D.

In contrast, the thickness δ of the lubrication film is much smaller than R. The relationship between δ, R and the capillary number is given by:[22,35]

$$\delta = 0.643(3\mathrm{Ca})^{2/3}R. \quad (2)$$

The thickness of the lubrication film is therefore between 13 and 96 nm, depending on the speed at which the colloidal suspension flows. This estimate is based on a purely hydrodynamic model and neglects other effects (disjoining pressure, wall roughness, *etc.*) which could influence the thickness δ.[36] Nevertheless, δ is expected to remain small compared to the other length scales of the problem.

Typical snapshots of bubble coverage are displayed in Fig. 4. Two main behaviors are observed, depending on the size of the beads: while the smaller particles (0.5 and 1 μm) are efficient in coating the interface, independently of the bubble speed, the 4.5 μm particles display a much weaker coating efficiency. The reason is that aggregates of particles of size 0.5 and 1 μm are small enough to enter into the gutters, but aggregates of two or more 4.5 μm particles are too large to flow through the gutters. Once a small aggregate is stuck at one of the gutters, successive particles are filtered out and blocked from reaching the interface, leading to the formation of large aggregates.

4.3 Influence of the flow speed

Finally we investigate the effect of flow speed on particle adsorption, focusing on experimens with 0.5 and 1 μm particles. For this we estimate the number of adsorbed particles from kymographs, such as the one shown in Fig. 2I and Fig. S5 (ESI†), which reveal that the fluorescence intensity directly downstream of the bubble is smaller than upstream of the bubble. This is a consequence of particle capture by the interface, since the colloids that adsorb onto the interface are removed from the bulk flow. We may therefore define the ratio $\phi = (I_u - I_d)/I_u$, where I_d and I_u represent the fluorescence intensities downstream and upstream of the bubble, respectively. The value of ϕ is a measure of the amount of colloids adsorbed onto the bubble interface.

The value of ϕ for different flow rates is shown on Fig. 5. For 0.5 μm particles, ϕ displays a non-monotonic dependence on the flow rate, while remaining at values below 15% (Fig. 5A). In contrast, for 1 μm particles ϕ displays a maximum value at low flow rates, decreasing to a plateau at high flow rate values, as shown in Fig. 5B. The absolute values of ϕ for these particles are in the range of 35 to 75%.

4.4 Final surface coverage

While ϕ measures the amount of particles captured by the bubble, a complementary measurement is the relative bubble area covered by the particles for each condition. This quantity is measured by releasing the bubble into the conical observation chamber, where it adopts a spherical shape with radius R_0. Then by increasing the ambient pressure, the bubble can be shrunk until the particles on the interface form a jammed state at a final bubble radius R_f (see Fig. S6, ESI†).[25]

The particle coverage of the interface in the coating channel can therefore be defined as:

$$\text{coverage} = \frac{A_f}{A_0} \times 100\%, \quad (3)$$

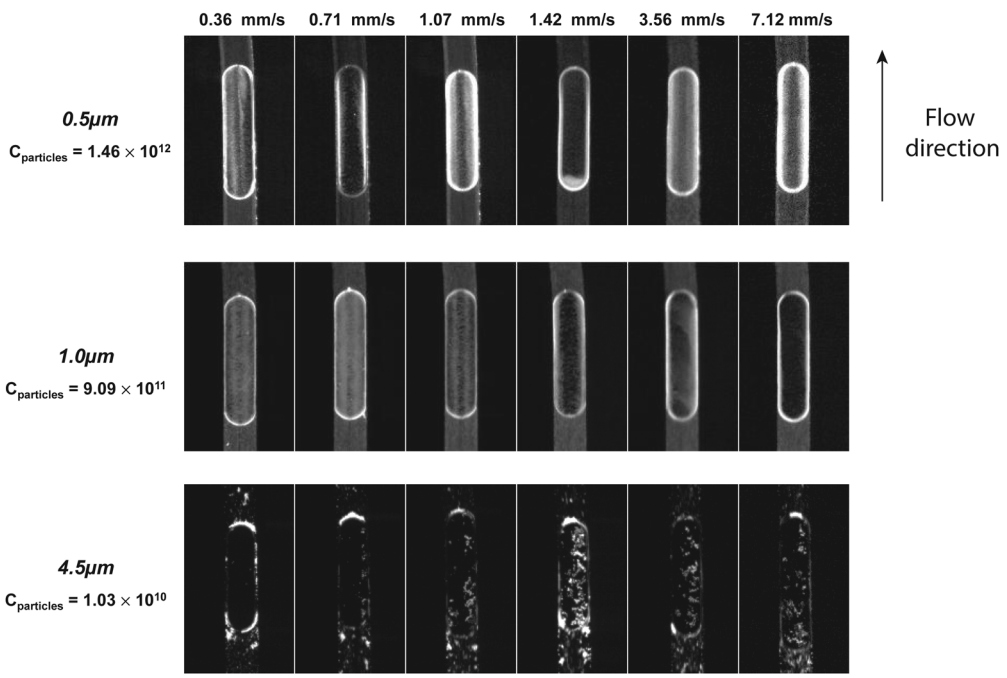

Fig. 4 Bubble coverage in the channel at position E from Fig. 2, for particles of different diameters and various flow speeds. Bubbles get coated by particles or aggregates small enough to enter into the 9 μm-gutters. Particles of 0.5 and 1.0 μm uniformly coated the bubble interface. Aggregates of 4.5 μm particles were too large to enter into the gutters, and could not coat the bubble efficiently.

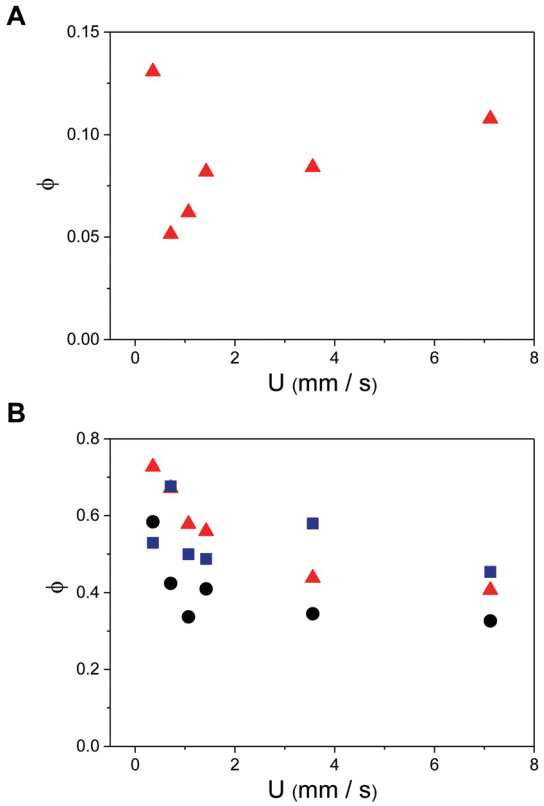

Fig. 5 (A) The fraction $\phi = (I_u - I_d)/I_u$ of adsorbed particles at the interface shows no clear dependence with the speed of the colloidal suspension for 0.5 μm particles. (B) For 1 μm particles, ϕ decreases when the speed of the colloidal suspension increases, except at the highest colloidal concentration. Concentration of the colloidal suspension: 0.1 wt% (▲), 0.5 wt% (●) and 0.8 wt% (■).

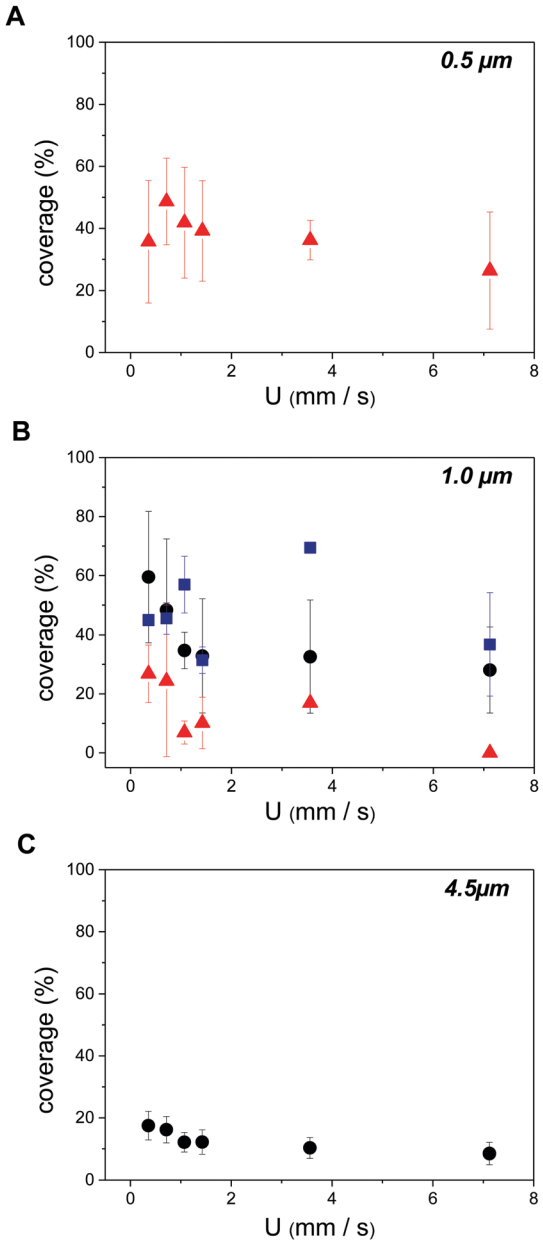

Fig. 6 Percentage coverage of the bubble interface as a function of the fluid velocity for (A) 0.5 μm, (B) 1.0 μm and (C) 4.5 μm particles. For 1.0 μm colloids, the particle concentration was varied between 0.1 wt% (▲), 0.5 wt% (●) and 0.8 wt% (■). No dependence of the coverage on the flow speed can be observed for 0.5 μm particles. Coverage decreases with increased flow speed for 1.0 and 4.5 μm particles.

where $A_f = 4\pi R_f^2$ is the surface area of the jammed bubble and $A_0 = 4\pi R_0^2$ is the surface area of the bubble before pressure increase. The evolution of surface coverage with particle size, particle concentration, and flow speed, is summarized in the plots in Fig. 6.

For 0.5 μm particles at a concentration of 0.1 wt% (Fig. 6A), the bubble interface was covered on average at 40% at the end of the coating channel and no clear dependence between the surface coverage and the fluid velocity could be observed. Increasing the concentration of particles to 0.5 wt% led to a qualitatively different behavior: as the bubble flowed within the channel, the available interface became entirely coated with particles before reaching the observation chamber. This induced the formation of a neck, and eventually to the break-up of the coated bubble into two bubbles, similarly to what was reported by Kotula and Anna[22] (see Fig. S7 and Movies 3, 4, ESI†).

For 1.0 μm particles, increasing the flow rate reduced the bubble coverage, as seen in Fig. 6B. At a concentration of 0.1 wt%, the coverage varied between almost none at all, for the highest speed, to 25% for the slowest speed. At higher particle concentrations, the average coverage increased, with a similar dependence on the flow speed: higher flow speeds led to worse coverage.

Finally for 4.5 μm particles, the surface coverage was always below 20%, as shown in Fig. 6C. The highest coverage occurred at the lowest flow speed, and coverage went down as the flow speed was increased. At all speeds, aggregates of 4.5 μm particles were too large to pass through the gutters, leading to poor coverage. Note that the final surface coverage observed in the conical observation chamber is consistent with the local adsorption dynamics reported on Fig. 5A and B.

4.5 Discussion

The results described above contradict what is expected when considering solely the flux of particles towards the bubble.

Indeed, the flux J of particles towards the bubble is proportional to the particle concentration c and to the relative speed Δv between the bubble and the fastest particles in the flow: $J \propto c\Delta v$. The relative speed Δv is fixed by the channel geometry and, in our case, $\Delta v \approx 0.8U$ for the fastest particles, where U is the mean flow speed (see Fig. S1, ESI†). Therefore, the particle flux should be larger at larger flow speeds, leading to an increased coverage when the flow speed increases. In contrast, we observed a decreasing coverage with increasing flow speed for 1 μm particles, and a non-monotonic relationship between coverage and flow speed for 0.5 μm particles.

This contradiction implies that the rate of adsorption is limited by a different mechanism than simply the transport of particles past the bubble. A possible source of limitation is the time spent by a particle in the gutters T_{gutter}, compared with the time T_{diff} required to approach the interface by diffusion. T_{gutter} is given by $T_{\text{gutter}} = l_b/(v_{\text{gutters}} - v_{\text{bubble}})$, where l_b is the length of the bubble, and v_{gutters} is the speed of a particle in the gutters. From the experimental movies, we estimate $v_{\text{gutters}} \approx 5v_{\text{bubble}}$ (see Movies S1 and S2, ESI†). This leads to a time spent in the gutters between $35 < T_{\text{gutter}} < 800$ ms for the fastest to the slowest bubbles, respectively. The diffusive time to cross the size a of the gutter is $T_{\text{diff}} \approx a^2/D$, where D is the diffusion coefficient of the particles. We find $D \approx 10^{-12}$ m^2 s^{-1} using the Stokes–Einstein equation, yielding $T_{\text{diff}} \approx 80$ s. Therefore, only a small fraction of the particles in the gutters could diffuse to the interface in a time T_{gutter}.

Given the inability of particles to cross the gutters during the advection time, we therefore assume that only the particles that are initially very close to the bubble will adsorb for the higher flow velocities. At lower flow velocities however, $T_{\text{gutter}} \approx 1$ s, which is about the time for a 1 μm particle to diffuse across its own size. This would increase the zone of capture of particles by about 1 particle diameter and would be consistent with the doubling of ϕ at the lowest values of U. Such a transport-limited scenario is consistent with the observed trends for 1 μm particles but should be verified by further experiments.

The evolution of the fraction of adsorbed particles with the flow speed shows no clear trend both for 0.5 μm particles at 0.1 wt%, and for 1 μm particles at 0.8 wt%, see Fig. 5. These two mass concentrations correspond to the highest number density of particles (see Table 1). In this case, it is possible that the crowding of the interface modifies the transport and the ability for new particles to adsorb on the already-crowded interface.

5 Adsorption in the lubrication films

Up to now we have solely considered the adsorption of particles flowing through the gutters. Yet, particles can sediment onto the floor of the microchannel, where they remain stationary in the presence of a mean flow. As the bubble arrives over these sedimented particles, they get pulled into the bottom lubricating film between the bubble and the wall and are finally adsorbed onto the interface at the back of the bubble, in a similar mechanism as what was described by Zoueshtiagh *et al.*[24] The particles then circulate and get redistributed along the interface, carried by the interfacial flow.

The adsorption in the lubrication film was investigated by favoring particle aggregation and sedimentation in the experiments, namely by keeping the fluids stationary for 1–30 min before the bubble was pushed through the coating channel. During this waiting period the individual particles formed aggregates, whose size increased with the waiting time, and that sedimented to the floor faster than individual particles would. After this waiting time the experiment was performed, as above, by flowing the bubble through the coating channel, and the interfacial coverage was measured when the bubble was released in the observation chamber at the end of the coating channel.

The evolution of the interfacial coverage with the waiting time is plotted on Fig. 7, for both 1 and 4.5 μm particles. Flow speed in the coating channel was kept at 3.56 mm s^{-1}, a value at which adsorption was sub-optimal in the absence of sedimentation. As seen on Fig. 7, the presence of aggregates always enhanced interfacial coverage. For 4.5 μm particles and in the absence of aggregation, only ~10% of the bubble interface was covered at the end of the coating channel. As the waiting time was increased and larger aggregates formed, the coverage increased and reached a plateau for waiting times larger than 5 minutes. In the plateau region, 40% of the interface was covered with particles, therefore increasing the coverage by a factor of 4 compared to the no-aggregation condition. For 1 μm particles, the effect was even more spectacular: as the waiting time increased from 0 to 5 minutes, surface coverage increased from 20 to 100% (see Fig. 7). Increasing the waiting time further led to the break-up of the coated bubble into two bubbles, an indication that the

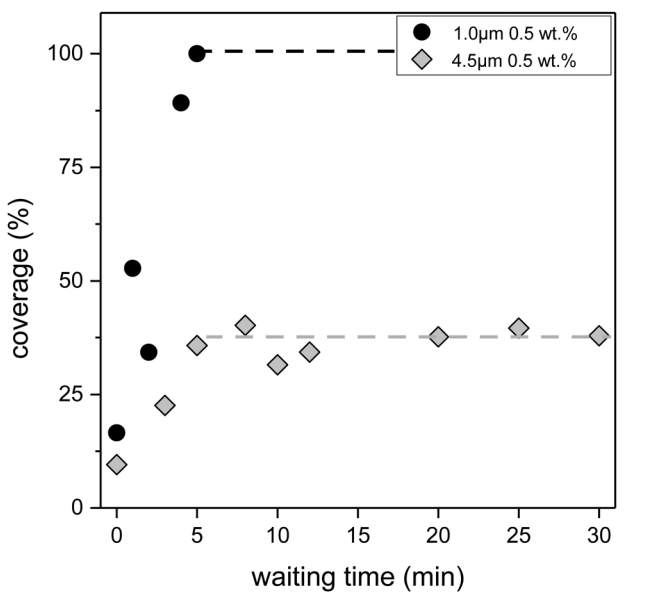

Fig. 7 Effect of aggregation on surface coverage. Particles were allowed to aggregate and sediment on the channel floor for times ranging from 1 to 30 minutes. Then, the air bubble was pushed through the coating channel. Flow speed: U = 3.56 mm s^{-1}. Interfacial coverage greatly increased as aggregates formed, both for 1 and 4.5 μm particles. Dashed lines show the maximal coverage obtained.

surface was extensively covered before reaching the observation chamber.

6 Summary and conclusion

In this study we explore the dynamics of particle adsorption at an air–liquid interface, as the bubble is transported by a colloidal suspension in a microchannel. The first question that we address is the relative velocity of the bubble and the outer flow. Our measurements of bubble velocity are in agreement with these previous results that indicate that bubbles should travel at the mean speed of the carrier fluid.[29–31] Nevertheless the particles flow past the bubbles in the gutters, suggesting that the bubble velocity is in fact slower than the mean flow in reality. This contradiction can be explained by noting that the ratio of cross-sectional area between the gutters and the microchannel amplifies any velocity differences. A simple geometric calculation gives an amplification factor of 70, indicating that even a velocity difference of a few percent will lead to a strong flow of particles in the gutters. Moreover, we observe that the presence of adsorbed particles at the interface does not influence the speed of the bubble, contrary to the strong effect of surfactants that reduce the bubble speed.[31]

We then identify two complementary mechanisms to cover the bubble interface. In the first mechanism, particles are adsorbed as they pass through the gutters formed between the interface and the channel corners (Movies S1 and S2 (ESI†) and Fig. 3A). In this condition, particles adsorb from the upstream direction and the coverage seems limited by the time required for the colloids to diffuse towards the interface rather than the flux of particles carried past the bubble by the outer fluid. This hypothesis is supported by the fact that the coverage is best at low flow rates (Fig. 5B), even though the flux of particles towards the bubble is lower at low flow rates than at high flow rates. Once the particles are sufficiently close to the interface, the flow profile can transport them to the front of the bubble where they are trapped either directly on the interface or in the lubrication film.

It is important to note that the particular flow patterns of microfluidic flows play a major role in the bubble and particle behaviors in our experiments, in contrast with unconfined flows such as in froth flotation where particles can move freely around the bubble.[9–13,15–18] For instance the confinement in microfluidics sets an upper limit on the size of individual particles that can reach the interface: particles with a size comparable to the gutter size jam at the entrance of the gutters and cannot flow through them. In contrast, in a froth flotation experiment, increasing the particle size leads to an enhanced surface coverage because of favorable hydrodynamic and inertial interactions.[9] Moreover, the interactions between advective and diffusive particle transport in a complex flow pattern, in addition to the presence of the walls, complicate the comparison of time scales with the classical contact time of froth flotation studies.

Finally, when particles are too large to pass through the gutters we observe a second coating mechanism that relies on the adsorption of particles initially sedimented at the channel floor. The effect can be enhanced by waiting for a few minutes before flowing the bubbles, thus allowing the particles to form larger sedimented aggregates. Then as the bubble passes by, colloids on the wall get trapped in the lubrication film between the bubble and the wall, eventually being caught at the back of the bubble. Even though the aggregates are usually three-dimensional, images captured during the bubble passage show that the interface flattens them into a two-dimensional layer, therefore ending up with a monolayer coverage of the bubble. The presence of aggregates has already been shown to enhance surface coverage in traditional froth flotation setups, which has typically been explained by the increased effective size of the particles, enhancing collision.[9,37–39] The mechanism shown here proposes a complementary process, where the presence of boundaries plays an important role.

Conflicts of interest

There are no conflicts to declare.

Acknowledgements

The authors thank Caroline Frot and Nicolas Taccoen for technical assistance. Part of this work was funded by the European Research Council (ERC) under Grant Agreement 278248 "Multicell". The image for the graphical abstract was kindly provided by Julien Husson.

References

1 W. Ramsden, *Proc. R. Soc. London*, 1903, **72**, 156–164.
2 S. U. Pickering, *J. Chem. Soc., Trans.*, 1907, **91**, 2001–2021.
3 S. Tcholakova, N. Denkov and A. Lips, *Phys. Chem. Chem. Phys.*, 2008, **10**, 1608–1627.
4 A. Maestro, E. Rio, W. Drenckhan, D. Langevin and A. Salonen, *Soft Matter*, 2014, **10**, 6975–6983.
5 D. Z. Gunes, M. Murith, J. Godefroid, C. Pelloux, H. Deyber, O. Schafer and O. Breton, *Langmuir*, 2017, **33**, 1563–1575.
6 D. Z. Gunes, O. Schafer, H. Chisholm, H. Deyber and C. Pelloux, *Lipid based foam*, *Eur. Pat.*, WO/2016/150978, 2016, pp. 1–10.
7 P. Pieranski, *Phys. Rev. Lett.*, 1980, **45**, 569.
8 R. Aveyard, B. P. Binks and J. H. Clint, *Adv. Colloid Interface Sci.*, 2003, **100–102**, 503–546.
9 A. V. Nguyen, R. J. Pugh and G. J. Jameson, in *Colloidal Particles at Liquid Interfaces*, ed. B. P. Binks and T. S. Horozov, Cambridge University Press, Cambridge, 2006, pp. 328–382.
10 Z. Dai, D. Fornasiero and J. Ralston, *Adv. Colloid Interface Sci.*, 2000, **85**, 231–256.
11 K. L. Sutherland, *J. Phys. Colloid Chem.*, 1948, **52**, 394–425.
12 B. Derjaguin and S. Dukhin, *Prog. Surf. Sci.*, 1993, **43**, 241–266.
13 D. Reay and G. A. Ratcliff, *Can. J. Chem. Eng.*, 1973, **51**, 178–185.

14 G. Collins and G. Jameson, *Chem. Eng. Sci.*, 1977, **32**, 239–246.
15 A. V. Nguyen, *Int. J. Miner. Process.*, 1999, **56**, 165–205.
16 A. V. Nguyen, P. George and G. J. Jameson, *Chem. Eng. Sci.*, 2006, **61**, 2494–2509.
17 Z. Brabcová, T. Karapantsios, M. Kostoglou, P. BasaÅŹová and K. Matis, *Colloids Surf., A*, 2015, **473**, 95–103.
18 P. Basařová, V. Machoň, M. Hubička and D. Horn, *Int. J. Miner. Process.*, 2010, **94**, 58–66.
19 A. B. Subramaniam, M. Abkarian, L. Mahadevan and H. A. Stone, *Langmuir*, 2006, **22**, 10204–10208.
20 A. B. Subramaniam, C. Mejean, M. Abkarian and H. A. Stone, *Langmuir*, 2006, **22**, 5986–5990.
21 A. B. Subramaniam, M. Abkarian and H. A. Stone, *Nat. Mater.*, 2005, **4**, 553–556.
22 A. P. Kotula and S. L. Anna, *Soft Matter*, 2012, **8**, 10759–10772.
23 Y. E. Yu, S. Khodaparast and H. Stone, *Soft Matter*, 2017, 1–10, in press.
24 F. Zoueshtiagh, M. Baudoin and D. Guerrin, *Soft Matter*, 2014, **10**, 9403–9412.
25 N. Taccoen, F. Lequeux, D. Z. Gunes and C. N. Baroud, *Phys. Rev. X*, 2016, **6**, 011010.
26 D. T. Eddington, J. P. Puccinelli and D. J. Beebe, *Sens. Actuators, B*, 2006, **114**, 170–172.
27 J. Schindelin, I. Arganda-Carreras, E. Frise, V. Kaynig, M. Longair, T. Pietzsch, S. Preibisch, C. Rueden, S. Saalfeld and B. Schmid, *et al.*, *Nat. Methods*, 2012, **9**, 676–682.
28 R. Dangla, S. C. Kayi and C. N. Baroud, *Proc. Natl. Acad. Sci. U. S. A.*, 2013, **110**, 853–858.
29 S. Jakiela, S. Makulska, P. M. Korczyk and P. Garstecki, *Lab Chip*, 2011, **11**, 3603.
30 S. Jakiela, P. M. Korczyk, S. Makulska, O. Cybulski and P. Garstecki, *Phys. Rev. Lett.*, 2012, **108**, 134501.
31 M. J. Fuerstman, A. Lai, M. E. Thurlow, S. S. Shevkoplyas, H. A. Stone and G. M. Whitesides, *Lab Chip*, 2007, **7**, 1479–1489.
32 R. Luo and L. Wang, *Chem. Eng. Res. Des.*, 2012, **90**, 998–1010.
33 R. Luo and L. Wang, *Microfluid. Nanofluid.*, 2012, **12**, 581–595.
34 H. Kinoshita, S. Kaneda, T. Fujii and M. Oshima, *Lab Chip*, 2007, **7**, 338–346.
35 H. Wong, C. Radke and S. Morris, *J. Fluid Mech.*, 1995, **292**, 71–94.
36 A. Huerre, V. Miralles and M.-C. Jullien, *Soft Matter*, 2014, **10**, 6888–6902.
37 W. Sun, M. J. Deng and Y. H. Hu, *Min. Sci. Technol.*, 2009, **19**, 483–488.
38 W. S. Ng, R. Sonsie, E. Forbes and G. V. Franks, *Miner. Eng.*, 2015, **77**, 64–71.
39 X. Zhang, Y. Hu, W. Sun and L. Xu, *Minerals*, 2017, **7**, 52.